10-2007

Fundamental emission via wave advection from a collapsing wave packet in electromagnetic strong plasma turbulence

Frederick A. Jenet
The University of Texas Rio Grande Valley

A. Melatos
University of Melbourne

P. A. Robinson
University of Sydney

Fundamental emission via wave advection from a collapsing wave packet in electromagnetic strong plasma turbulence

Cite as: Phys. Plasmas **14**, 100702 (2007); https://doi.org/10.1063/1.2787500
Submitted: 19 March 2007 . Accepted: 31 August 2007 . Published Online: 19 October 2007

F. A. Jenet, A. Melatos, and P. A. Robinson

Fundamental emission via wave advection from a collapsing wave packet in electromagnetic strong plasma turbulence

F. A. Jenet
Department of Physics and Astronomy, University of Texas at Brownsville, Brownsville, Texas 78520, USA

A. Melatos
School of Physics, University of Melbourne, Parkville, VIC 3010, Australia

P. A. Robinson
School of Physics, University of Sydney, Sydney NSW 2006, Australia

(Received 19 March 2007; accepted 31 August 2007; published online 19 October 2007)

Zakharov simulations of nonlinear wave collapse in continuously driven two-dimensional, electromagnetic strong plasma turbulence with electron thermal speeds $v \geqslant 0.01c$ show that for $v \leqslant 0.1c$, dipole radiation occurs near the plasma frequency, mainly near arrest, but for $v \gtrsim 0.1c$, a new mechanism applies in which energy oscillates between trapped Langmuir and transverse modes until collapse is arrested, after which trapped transverse waves are advected into incoherent interpacket turbulence by an expanding annular density well, where they detrap. The multipole structure, Poynting flux, source current, and radiation angular momentum are computed. © *2007 American Institute of Physics*. [DOI: 10.1063/1.2787500]

Electromagnetic (EM) radiation is generated at the plasma frequency ω_p and its harmonics by nonlinearly collapsing wave packets in strong plasma turbulence (SPT), via various mechanisms. It is observed, or likely to be seen, in beam-plasma and ionospheric-heating experiments,[1–3] pending inertial confinement and laser-plasma experiments such as the Laser Megajoule (LMJ) experiment and National Ignition Facility (NIF),[4] and possibly pulsar radio emission,[5] in the SPT regime $W=\epsilon_0\langle|\mathbf{E}|^2\rangle/4n_0k_BT_e \gtrsim (k\lambda_D)^2$, where $\langle|\mathbf{E}|^2\rangle^{1/2}$ is the rms electric field strength, n_0 is the mean electron density, T_e is the electron temperature, k is the characteristic electrostatic (ES) wavenumber, and λ_D is the Debye length. Further situations in which EMSPT and related EM emission are likely to occur include solar flares, astrophysical jets, and active galactic nuclei, with electron thermal speeds $v \gtrsim 0.1c$.[6]

Nonlinear collapse of ES Langmuir (L) waves proceeds via nucleation, ponderomotive self-focusing, and arrest by transit-time damping.[3,7,8] Less is known of nonlinear collapse of a coupled system of L and T (transverse EM) waves. Spectra have been measured during collapse for a range of driver parameters in beam-plasma and ionospheric-heating experiments;[1,2] simulations of undriven EMSPT have reproduced features of these data.[5,9,10] Analytic results include wave equations governing EMSPT and proofs of collapse by virial methods.[11] Some estimates of ω_p emission have been made using the dipole approximation.[11–13]

In this Letter, we investigate EM emission near ω_p by nonlinearly collapsing wave packets in two-dimensional (2D) EMSPT, and other properties of these packets. At high electron temperatures ($v \gtrsim 0.1c$, i.e., $T_e \gtrsim 60$ MK) we also report a new emission mechanism. We perform numerical simulations on a 256^2 grid, which produce a turbulent state with $\gtrsim 10^2$ wave packets in the simulation box, cover a wide range of electron thermal speeds $0.01c \leqslant v=(k_BT_e/m_e)^{1/2} \leqslant 0.57c$ (60 MK $\lesssim T_e \lesssim$ 2000 MK), and are continuously driven to a statistically steady state. Until recently, numerical work was restricted to a 64^2 grid containing $\leqslant 3$ packets in an undriven case at $v=0.08c$.[9] Analytic work was restricted to the regime $v \ll c$, where back-reaction of T waves on collapse dynamics is slight.[12,13] The overall T_e range investigated covers many of the experiments above, while the new emission mechanism (along with existing ones) is potentially relevant to upcoming high-temperature experiments such as NIF and LMJ, and the astrophysical applications mentioned.

EMSPT is described by the Zakharov equations:[3,11] an L-T wave equation for the field envelope $\mathcal{E}(\mathbf{x},t)$,

$$i\frac{\partial\mathcal{E}}{\partial t}=\left(\frac{v_T^2}{2\omega_p}\nabla\times\nabla\times-\frac{v_L^2}{2\omega_p}\nabla\nabla\cdot+\frac{\omega_p\delta n}{2n_0}-i\hat{\gamma}_L\right)\mathcal{E}, \quad (1)$$

defined by $\mathbf{E}=\mathcal{E}e^{-i\omega_pt}$, and an ion-sound ($S$) wave equation for the slowly varying, ion sound-like quasineutral density perturbation $\delta n(\mathbf{x},t)$,

$$\left(\frac{\partial^2}{\partial t^2}+2\hat{\gamma}_S\frac{\partial}{\partial t}-v_S^2\nabla^2\right)\frac{\delta n}{n_0}=\frac{\epsilon_0}{4n_0m_i}\nabla^2(|\mathcal{E}|^2), \quad (2)$$

with $v_S^2=(1+3T_i/T_e)(m_e/m_i)v^2$, $v_L^2=3v^2(1+\xi/5)/(1+5\xi+\xi^2)$, $v_T^2=c^2(1+6\xi+6\xi^2/5)/(1+5\xi+\xi^2)$, $\omega_p^2=(n_0e^2/m_e\epsilon_0)(2+\xi)/(2+6\xi+3\xi^2)$, and $\xi=v^2/c^2$. We approximate the exact relativistic expressions for v_L and v_T by two-point Padé formulas,[14] but neglect relativistic ponderomotive terms, which tend to be much smaller than those retained. (The results are semiquantitative due to this neglect and the approximations inherent in the Zakharov equations, which neglect higher harmonics and thus also require $k^2v_T^2, k^2v_L^2 \ll \omega_p^2$.) The operators $\hat{\gamma}_L(\mathbf{x},t)$ and $\hat{\gamma}_S(\mathbf{x},t)$ describe Langmuir and ion-sound damping and growth; the T modes are not damped/driven directly and there is no ambient magnetic field. We solve Eqs. (1) and (2) using a spectral code with periodic boundary conditions, constant negative-damping driver at $k=0$, transit-time damping at high k,[3,8,10] and low ion-sound damping ($T_i/T_e=0.01$) to avoid suppressing cou-

pling between S and T modes.[15] Driver/damping parameters are as in Ref. 10. The negative-damping driver is chosen for simplicity to provide energy to the turbulence. Alternatives such as short-wavelength driving by beams can yield energy-cascade emission features in addition to the collapse-related ones described here, while $k=0$ fixed-amplitude "clamp"-field drives can be applied at frequencies near ω_p, delivering energy directly to trapped states in some cases. These effects are essential in many applications, especially if including decay cascades and emission before collapse. They can even forestall collapse in some cases, e.g., by preventing the buildup of a low-k condensate. However, if collapse occurs, it and subsequent burnout and early relaxation are relatively unaffected by these considerations[3] so we could equally well have initialized undriven packets to collapse in the present study, which focuses only on collapse-generated ω_p emission.

Simulations show that fully developed EMSPT has a two-component spatial structure of low-level, incoherent, delocalized waves (free modes) punctuated by intense, coherent wave packets (trapped modes).[10] Packets form by nucleation: wavenumber-matched L and T modes are trapped in a preexisting, relaxed density well ($k_{L,T} \approx k_S$). When the energy density exceeds the threshold for collapse, $W \sim (k_L \lambda_D)^{-2}$, the refractive term $\delta n \propto |\mathcal{E}|^2$ in Eq. (1) exceeds the dispersive $\nabla\times\nabla\times$ and $\nabla\nabla\cdot$ terms, and the packet collapses to short scales and high fields on a time scale comparable to the plane-wave modulational instability, $t_c \sim (\omega_p W)^{-1}$. For $v \lesssim 0.1c$, the L mode collapses independently, as in electrostatic SPT, emitting free T modes like an antenna,[3,10] but for $v \gtrsim 0.1c$ the L and T modes remain coupled during collapse, with length scales in a constant ratio.[10] Each regime applies to some of the applications mentioned above.

Figure 1(a) shows the geometry of a single wave packet near arrest, extracted from a fully developed SPT ensemble with $v=0.57c$.[10] The life cycle of an extracted packet is more realistic than that of an isolated packet with noiseless, symmetric initial conditions as previously simulated. Numerically decomposing the trapped fields into 2D multipole components, $\Phi^{(m)} \propto e^{im\phi}$, shows they are predominantly dipolar, with $\mathcal{E}_L = -\Sigma_{m=\pm1} \nabla \Phi_L^{(m)}$, $\mathcal{E}_T = \hat{\mathbf{z}} \times \Sigma_{m=\pm1} \nabla \Phi_T^{(m)}$, $\Phi_{L,T}^{(\pm1)} \propto (1 + r^2/a_{L,T}^2)^{-1} r e^{\pm i\phi}$, $a_L \approx a$, and $a_T \approx (c/v)^{0.7} a$, where a is the length scale of the density well.[10] This field structure is roughly preserved throughout collapse; the monopole components $\Phi_{L,T}^{(0)}$ increase as collapse proceeds but remain modest, with $|\Phi_{L,T}^{(0)}| \lesssim 0.2 |\Phi_{L,T}^{(\pm1)}|$ at all times. For the L waves, this agrees with previous results.[16]

Generation of dipole radiation at ω_p is weak during collapse (it has been argued it is forbidden in some limits by $\mathbf{k}$ conservation[12]). But $L \to T$ conversion does occur, especially near arrest when ion inertia is significant ($|\delta n| \approx 0.3 n_0$), and seen experimentally.[1,9] A similar mechanism operates for $v = 0.01c$, except the T waves are free, near-plane eigenmodes, with $|\Phi_{L,T}^{(0)}| \approx |\Phi_{L,T}^{(\pm1)}| \approx |\Phi_{L,T}^{(\pm2)}|$, clumped on the scale $a_T \gg a_L$. There is weak association of clumps of T waves with density wells, a possible *in situ* diagnostic for this mechanism.[10]

The density well in Fig. 1(a) is approximately circular with $\delta n^{(0)} \propto (1 + r^2/a^2)^{-2}$.[10] Its quadrupole component satisfies $\delta n^{(\pm2)} \approx 0.1 \delta n^{(0)}$ at the center and $\delta n^{(\pm2)} \approx \delta n^{(0)}$ in the wings ($r \gtrsim 2a$). This structure is consistent with $\delta n \propto |\mathcal{E}|^2$ for subsonic collapse ($\partial_t^2 \ll v_S^2 \nabla^2$), as $\mathcal{E}$ is approximately dipolar. Consequently, energy is not transferred between trapped electric-field eigenstates of unequal m, except for weak $|\Delta m| = 2$ transitions, because the time-dependent part of the operator $\hat{Z}$ in Eq. (1), $i\partial_t |\,\rangle = \hat{Z} |\,\rangle$, has $\hat{Z} \propto \delta n \approx \delta n^{(0)}$, where $|\,\rangle$ denotes an electric field eigenstate in Dirac notation. In contrast, trapped modes couple to free T modes since $\langle \pm1, L | \hat{Z} | T, \mathbf{k} \rangle \neq 0$, where this notation denotes the overlap integral between an $m = \pm1$ trapped L eigenstate and a plane wave T state of wave vector $\mathbf{k}$.

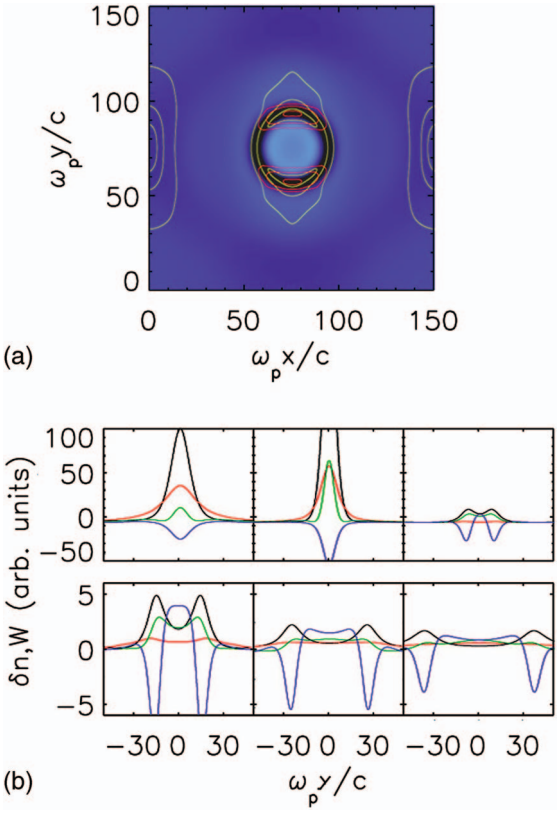

FIG. 1. (Color) (a) Packet with $v=0.57c$ just after arrest, showing the annular well δn (bluescale; dark negative, light positive, ranging from about -0.4 to $0.1W$) and ES and EM energy densities W_L (yellow) and W_T (red). The $|m|=0,1,2$ components were fitted and the packet resulting from these was plotted to reduce noise, thus introducing artificial spatial periodicity. (b) Cross sections along the y axis at successive times, showing δn (blue), W_T (red), W_L (green), and W (black).

The escape of T modes at ω_p from a collapsing packet is illustrated in Fig. 1(b), where successive cross sections of the density well and trapped electric fields are plotted transverse to the L dipole axis. In the first two snapshots, during subsonic collapse, trapped L and T modes contract to short scales and high fields self-similarly in a circular well $\delta n \propto |\mathcal{E}|^2$, with $a_T/a_L \approx$ const. In the third snapshot, near arrest, the well transforms from having a single central minimum into an expanding annulus. An analog of this radiated S pulse was observed in simulations of clamp-driven ESSPT for $T_i \ll T_e$,[15] but it was not annular; the well became peanut-shaped at arrest and the S pulse emerged preferentially along the minor axis.[3] In contrast, in EMSPT, the crossed L and T

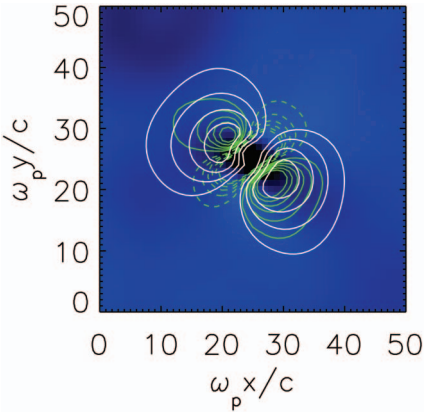

FIG. 2. (Color) Radiation from a packet with $v=0.1c$, showing current source $|\nabla\times\mathcal{J}|$ (white contours), divergence of Poynting flux $\nabla\cdot\mathbf{S}_P$ (green contours; dashed negative, solid positive), and δn (bluescale as in Fig. 1).

dipoles, whose amplitudes are comparable for $v=0.57c$, give a roughly isotropic total ponderomotive drive term, and the dispersive terms in $\hat{Z}$ approach ∇^2 (cf. $\nabla\nabla\cdot$ in ESSPT). In the fourth to sixth snapshots, after burnout, the annular well can be seen expanding, becoming shallower until $|\delta n|$ decreases to where the L and T modes detrap and propagate into the background turbulence. This advection of T waves into the background is fundamentally different from the antenna model of T-wave generation in the $v\leqslant 0.1c$ regime.[2,9,12,13] In subsequent propagation through the background, T waves scatter off overdense regions ($\omega_T<\omega_p$) and lose energy to damped Langmuir and ion-sound waves, mainly via $T\rightarrow L+S$, and linear mode conversion.[17]

Contours of $|\nabla\times\mathcal{J}|$ are displayed in Fig. 2, where $\mathcal{J}$ is the envelope of the source current $\mathbf{J}=\mathcal{J}e^{-i\omega_p t}$ of the transverse magnetic field $\mathbf{B}=\mathcal{B}e^{-i\omega_p t}$, with[9]

$$-2i\omega_p\partial_t\mathcal{B}-\omega_p^2\mathcal{B}-c^2\nabla^2\mathcal{B}=\epsilon_0^{-1}\nabla\times\mathcal{J}. \tag{3}$$

We observe that $|\nabla\times\mathcal{J}|$ exhibits two pronounced peaks of similar amplitude, centered on the bulges of the peanut-shaped W_T contours. There is no evidence for four peaks in $|\nabla\times\mathcal{J}|$, unlike previous undriven numerical simulations with $v=0.08c$, possibly because of the increasing isotropy with increasing v mentioned above.[9] Also $|\mathcal{J}|$ peaks near $|\nabla\times\mathcal{J}|$, but less sharply, and a peanut-shaped current halo surrounds the packet, of opposite sign to the peak $\mathcal{J}$. The phase of $\nabla\times\mathcal{J}$ determines the orientation and shape of the radiation pattern. We find empirically that the two peaks have arbitrary absolute phases, yielding randomly oriented packets, but their phases differ by $\approx\pi$ during collapse. To interpret these results, we solve Eq. (3) for a model slowly varying source $\epsilon_0^{-1}\nabla\times\mathcal{J}=[\sigma_1\delta(x-d)+\sigma_2\delta(x+d)]\delta(y)e^{-it/t_c}\hat{\mathbf{z}}$, with $d=0.5a_L$, amplitudes $\sigma_1=i\sigma_2$, and $\mathcal{B}(\mathbf{x},0)=0$. The result, $\mathcal{B}(\mathbf{x},t)=(2\pi)^{-2}\int d^2\mathbf{k}\exp(i\mathbf{k}\cdot\mathbf{x})\mathcal{B}(\mathbf{k},t)$, with

$$\mathcal{B}(\mathbf{k},t)=\frac{\sigma_1\exp(-ik_xd)+\sigma_2\exp(ik_xd)}{c^2k^2-\omega_p^2-2\omega_p/t_c}\times\{\exp(-it/t_c)-\exp[i(c^2k^2-\omega_p^2)t/2\omega_p]\}, \tag{4}$$

yields W_T contours similar to Fig. 1(a).

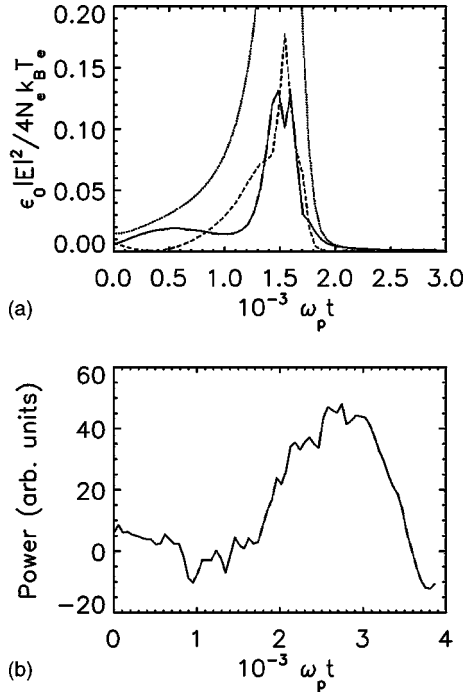

FIG. 3. (a) Energy densities W_L (dashed), W_T (solid), and $W=|\mathbf{E}_L+\mathbf{E}_T|^2$ (dotted), vs t. (b) Radiated power vs t, computed by integrating the outward component of $\mathbf{S}_P$ around a 128^2 square centered on the packet.

The Poynting flux (which is perpendicular to the 2D system) $\mathbf{S}_P=\mu_0^{-1}\mathcal{E}_T\times\mathcal{B}_T^*$ and $\nabla\cdot\mathbf{S}_P$ around a packet are plotted in Fig. 2. (We omit the "static," circulating term $\mu_0^{-1}\mathcal{E}_L\times\mathcal{B}_T^*$, although it is greater, because it does not track radiated energy and integrates to zero on a contour that encloses the packet.) For $v=0.1c$, $\nabla\cdot\mathbf{S}_P$ is quadrupolar, with its axis of symmetry usually oblique to the major axis of δn (cf. $\nabla\times\mathcal{J}$ in Fig. 2). EM energy flows in through the lobes in Fig. 2, but the packet is a source overall. In steady-state turbulence, about half the packets have $\nabla\cdot\mathbf{S}_P>0$ at their centers.

The spatial distribution of L and T damping can be studied using Fig. 2; L modes dissipate by transit-time damping, with $\partial_t W_L=\mathcal{E}_L\cdot\partial_t\mathcal{E}_L^*+\text{c.c.}$ and $\partial_t\mathcal{E}_L=-(2\pi)^{-2}\int d^2\mathbf{k}\times\exp(i\mathbf{k}\cdot\mathbf{x})\gamma_L(\mathbf{k})\mathcal{E}_L(\mathbf{k})$.[3] We find $\partial_t W_L<0$ integrated over the simulation box and every individual packet, as expected. However, regions with $\partial_t W_L>0$ exist in every packet, aligned perpendicular to the dipole axis, indicating that energy is redistributed within packets near arrest.[3,7,8] The T damping is indirect: T modes scatter off background density perturbations, coupling energy into damped L and S waves. We find some evidence of coincidence of regions with $\partial_t W_T+\nabla\cdot\mathbf{S}_P<0$ and overdense regions with $\omega_T<\omega_p$, but detailed study of this is beyond the scope of this Letter.

Figure 3 illustrates how the energy content of a collapsing packet evolves in fully developed SPT. During nucleation and subsonic collapse ($t<t_c\approx 2\times 10^3\omega_p^{-1}$), energy "sloshes" between trapped L and T modes, executing one cycle over the interval $t<t_c$ as in Fig. 3(a), where the two time series repeatedly cross. Typically, L waves nucleate first, with a small admixture of T waves, then energy passes from L to T modes as collapse proceeds. Simultaneously, energy sloshes between the $m=\pm 1$ harmonics. Mode sloshing does not occur in ESSPT; it arises because the L and T

modes execute coupled oscillations in a common, ponderomotive density well, with $\delta n=-\epsilon_0(|\mathcal{E}_L|^2+|\mathcal{E}_T|^2)/4m_iv_S^2$. In 1D, this is described by two nonlinear Schrödinger equations,

$$2i\omega_p\partial_t\mathcal{E}_T+c^2\partial_x^2\mathcal{E}_T=\omega_p^2\mathcal{E}_L\delta n/2n_0, \tag{5}$$

$$2i\omega_p\partial_t\mathcal{E}_L+3v^2\partial_x^2\mathcal{E}_L=\omega_p^2\mathcal{E}_T\delta n/2n_0, \tag{6}$$

whose solutions are mixed L-T modes between which energy cycles at a frequency $\Delta\omega$. To estimate $\Delta\omega$, we approximate each field E_C $(C=L,T,S)$ as a segment of plane wave $E_C \propto A_C\exp(ik_Cx-i\omega_Ct)$, with $A_S\propto\delta n/n_0$. Then Eqs. (5) and (6) imply the interactions select approximately matched wave numbers and give

$$(\Delta\omega/\omega_p)^2\approx(3k_L^2v^2-k_T^2c^2)^2/4\omega_p^4+(\delta n/2n_0)^2. \tag{7}$$

This estimate is only semiquantitative; better ones could be obtained by considering energy splitting between accurate eigenfunctions of the density well.

The power emitted by a collapsing packet into T waves, computed by integrating $\mathbf{S}_P$ around a contour enclosing the packet in fully developed SPT, is plotted in Fig. 3(b) versus t. We observe negligible emission during nucleation and collapse, then a burst after arrest. From nucleation to peak, W_T increases approximately tenfold, much less than the $\sim10^3$-fold increase seen in simulations starting with smooth, high-field initial conditions where a global plane-wave modulational instability occurred.[9] The burst is advected outwards by the expanding, annular density well in Fig. 1; its peak $(t=1.6\times10^3\omega_p^{-1})$ lags arrest $(t=2.6\times10^3\omega_p^{-1})$ by the ion-sound travel time from the center of the packet to the $\nabla\cdot\mathbf{S}_P$ integration contour. This is the first direct numerical evidence for such radiation transport in EMSPT. Radiation is emitted near the cutoff at ω_p, or at most at the plasma frequency corresponding to the enhanced-density well "rim" seen in Fig. 1, so propagation effects must be taken into account when comparing with observations; these include scattering, mode conversion, and reabsorption of the low-frequency part of the spectrum. One signature of our mechanism is the association between T waves and underdense regions, which will be more marked than for waves emitted further above ω_p, e.g., via decay. A qualitatively similar association exists for T waves in general, due to refraction, but the new mechanism must be included in general for quantitative agreement to be attained.

The angular momentum of a wave packet is

$$M_i=\frac{i\epsilon_0\epsilon_{ijk}}{4\omega_p}\int d^2\mathbf{x}[x_j(\mathcal{E}_l\partial_k\mathcal{E}_l^*-\mathcal{E}_l^*\partial_k\mathcal{E}_l)+2\mathcal{E}_j\mathcal{E}_k^*]+\frac{\epsilon_0\epsilon_{ijk}}{4n_0}\left\langle\int d^2\mathbf{x}\mathcal{E}\cdot\mathcal{E}^*x_j\partial_k(\delta n)\right\rangle, \tag{8}$$

where $\langle\,\rangle$ denotes an average over the ion-sound time scale. The first term in Eq. (8) is the sum of a field component, $\epsilon_0\mathbf{x}\times(\mathcal{E}\times\mathcal{B}^*)$, and a mechanical component, $n_em_e\mathbf{x}\times\mathbf{v}_e$, with $n_ev_e\propto\mathcal{E}\nabla\cdot\mathcal{E}^*$ (electron oscillations). The second term is due to electrons accelerated by ponderomotively driven ions, with $\partial_t\mathbf{v}_e\propto\nabla(\delta n+\epsilon_0|\mathcal{E}|^2/4m_iv_S^2)$. For a packet of the form $\Phi_{L,T}=A_{L,T}a_{L,T}(\alpha x+i\beta y)/(r^2+a_{L,T}^2)$, with $\alpha>\beta=(1-\alpha^2)^{1/2}$, the first term of M_z equals $2\pi\epsilon_0\alpha\beta A_{L,T}^2/3\omega_p$. Most packets have $\alpha\approx1$ (linearly polarized at the center),[3,16] so the first term in Eq. (8) is near zero in subsonic collapse. However, during burnout and any supersonic collapse phase immediately preceding it, the second term of M_z is expected to grow $(\delta n+\epsilon_0|\mathcal{E}|^2/4m_iv_S^2\neq0)$, while M_z is conserved. Hence the first term changes, as do α and the ellipticity and orientation of the W contours. We thus predict that a packet will elongate and rotate in the final stages of collapse, as angular momentum is carried off by S modes, due to associated redistributions of plasma density. Slight rotation in the outer contours of some packets is indeed seen. However, the transition to supersonic collapse only just begins as strong transit-time damping cuts in,[3] and dissipation of fields during burnout is very rapid,[3,8,18] so it is hard to see rotation in the packet centers, especially as δn and Φ are roughly circular there.

In summary, simulations of fully developed EMSPT for a range of temperatures reveal a number of features of EM emission near ω_p from collapsing packets, including the existence of a new high-temperature $(T\gtrsim60$ MK) radiation mechanism in which trapped EM waves are advected into the background turbulence by expanding post-collapse density wells, then detrapped. Key properties and structures of wave and density states have also been explored.

The NSF, NASA, Miller Institute for Basic Research in Science, Australian Research Council, and Caltech Center for Advanced Computing supported this work.

[1] D. A. Whelan and R. L. Stenzel, Phys. Rev. Lett. **47**, 95 (1981); P. Y. Cheung, A. Y. Wong, C. B. Darrow, and S. J. Qian, *ibid.* **48**, 1348 (1982); M. Schneider and M. Q. Tran, Phys. Lett. **91A**, 25 (1982).
[2] E. Mjølhus, A. Hansen, and D. F. DuBois, J. Geophys. Res. **100**, 17527, DOI:10.1029/95JA01158 (1995); P. Y. Cheung, E. Mjølhus, D. F. DuBois, J. Pau, H. Zwi, and A. Y. Wong, Phys. Rev. Lett. **79**, 1273 (1997).
[3] P. A. Robinson, Rev. Mod. Phys. **69**, 507 (1997), and references therein.
[4] S. V. Bulanov, T. Zh. Esirkepov, N. M. Naumova, F. Pegoraro, and V. A. Vshivkov, Phys. Rev. Lett. **82**, 3440 (1999); Y. Sentoku, T. Zh. Esirkepov, K. Mima *et al.*, *ibid.* **83**, 3434 (1999); K. Mima, M. S. Jovanović, Y. Sentoku, Z.-M. Sheng, M. M. Škorić, and T. Sato, Phys. Plasmas **8**, 2349 (2001); D. Umstadter, J. Phys. D **36**, R151 (2003).
[5] J. Weatherall, Astrophys. J. **483**, 402 (1997).
[6] D. N. Baker, J. E. Borovsky, G. Benford, and J. A. Eilek, Astrophys. J. **326**, 110 (1988).
[7] P. A. Robinson, Phys. Fluids B **1**, 490 (1989).
[8] P. A. Robinson, Phys. Fluids B **3**, 545 (1991).
[9] K. Akimoto, H. L. Rowland, and K. Papadopoulos, Phys. Fluids **31**, 2185 (1988).
[10] A. Melatos, F. A. Jenet, and P. A. Robinson, Phys. Plasmas **14**, 020703 (2007).
[11] J. Gibbons, S. G. Thornhill, M. J. Wardrop, and D. ter Haar, J. Plasma Phys. **17**, 153 (1977); M. Kono, M. M. Škorić, and D. ter Haar, *ibid.* **26**, 123 (1981); L. H. Li, Phys. Fluids B **5**, 350 (1993).
[12] H. P. Freund and K. Papadopoulos, Phys. Fluids **23**, 732 (1980); B. Hafizi and M. V. Goldman, *ibid.* **24**, 145 (1981).
[13] B. N. Brejzman and L. S. Pekker, Phys. Lett. **65A**, 121 (1978); V. V. Yan'kov, Sov. J. Plasma Phys. **8**, 48 (1982).
[14] A. Magneville, J. Plasma Phys. **44**, 191 (1990).
[15] G. D. Doolen, D. F. DuBois, and H. A. Rose, Phys. Rev. Lett. **54**, 804 (1985); D. Russell, D. F. DuBois, and H. A. Rose, *ibid.* **60**, 581 (1988).
[16] D. L. Newman, P. A. Robinson, and M. V. Goldman, Phys. Rev. Lett. **62**, 2132 (1989).
[17] P. A. Robinson and I. H. Cairns, Sol. Phys. **181**, 363 (1998).
[18] D. L. Newman, R. M. Winglee, P. A. Robinson, J. Glanz, and M. V. Goldman, Phys. Fluids B **2**, 2600 (1990).